



# Hydrogen production from plastic waste: A comprehensive simulation and machine learning study

Mohammad Lahafdoozian<sup>a</sup>, Hossein Khoshkroudmansouri<sup>a</sup>, Sharif H. Zein<sup>a,\*</sup>, A.A. Jalil<sup>b,c</sup>

<sup>a</sup> School of Engineering, Faculty of Science and Engineering, University of Hull (UoH), Kingston Upon Hull, HU6 7RX, UK

<sup>b</sup> Center of Hydrogen Energy, Institute of Future Energy, Universiti Teknologi Malaysia, 81310, UTM Johor Bahru, Malaysia

<sup>c</sup> Faculty of Chemical and Energy Engineering, Universiti Teknologi Malaysia, 81310, UTM Johor Bahru, Johor, Malaysia

## ARTICLE INFO

Handling Editor: Jinlong Gong

### Keywords:

Hydrogen production  
Aspen plus  
Optimization  
Modelling  
Machine learning

## ABSTRACT

Gasification, a highly efficient method, is under extensive investigation due to its potential to convert biomass and plastic waste into eco-friendly energy sources and valuable fuels. Nevertheless, there exists a gap in comprehension regarding the integrated thermochemical process of polystyrene (PS) and polypropylene (PP) and its capability to produce hydrogen (H<sub>2</sub>) fuel. In this study a comprehensive process simulation using a quasi-equilibrium approach based on minimizing Gibbs free energy has been introduced. To enhance H<sub>2</sub> content, a water-gas shift (WGS) reactor and a pressure swing adsorption (PSA) unit were integrated for effective H<sub>2</sub> separation, increasing H<sub>2</sub> production to 27.81 kg/h. To investigate the operating conditions on the process the effects of three key variables in a gasification reactor namely gasification temperature, feedstock flow rate and gasification pressure have been explored using sensitivity analysis. Furthermore, several machine learning models have been utilized to discover and optimize maximum capacity of the process for H<sub>2</sub> production. The sensitivity analysis reveals that elevating the gasification temperature from 500 °C to 1200 °C results in higher production of H<sub>2</sub> up to 23 % and carbon monoxide (CO). However, generating H<sub>2</sub> above 900 °C does not lead to a significant upturn in process capacity. Conversely, an increase in pressure within the gasification reactor is shown to decrease the system capacity for generating both H<sub>2</sub> and CO. Moreover, increasing the mass flow rate of the gasifying agent to 250 kg/h in the gasification reactor has shown to be merely productive in process capacity for H<sub>2</sub> generation, almost a 5 % increase. Regarding pressure, the hydrogen yield decreases from 22.64 % to 17.4 % with an increase in pressure from 1 to 10 bar. It has been also revealed that gasification temperature has more predominant effect on Cold gas efficiency (CGE) compared to gasification pressure and Highest CGE Has been shown by PP at 1200 °C. Among the various machine learning models, Random Forest (RF) model demonstrates robust performance, achieving R<sup>2</sup> values exceeding 0.99.

## 1. Introduction

The exploration of alternative and environmentally sustainable energy sources has gained significant attention from researchers due to the growing energy demand, global warming, and the increased consumption of fossil fuels [1]. To eliminate the heavy dependency on conventional fuels, there is a pressing need for the development of renewable and environmentally friendly fuel, and energy production techniques. Pyrolysis and gasification emerge as promising technologies in meeting these dual criteria, owing to their versatile application with diverse carbon-based resources [2].

Plastic has mainly replaced texture, wood, and ceramic in a variety of

industries due to low production cost and durability [3]. From 270 million metric tons (MMT) in 2000, global plastic production increased to 367 MMT in 2020, and predictions indicate that this upward trend is likely to be sustained, reaching 445 MMT by 2025 and 590 MMT by 2050 [4]. The utilization of plastics, despite their widespread demand, has been associated with potential environmental hazards due to their non-biodegradable nature [5]. The inability of plastics to decompose naturally has led to the aggregation of plastic waste in various ecosystems, leading to adverse effects on the environment [6]. These effects include the pollution of water resources and soil, the endangerment of wildlife, and the disruption of terrestrial and aquatic ecological balance leading to a significant disadvantage of plastic usage [7]. It has been shown that a notable amount of plastic waste generated globally,

\* Corresponding author.

E-mail address: [S.H.Zein@hull.ac.uk](mailto:S.H.Zein@hull.ac.uk) (S.H. Zein).

<https://doi.org/10.1016/j.ijhydene.2024.01.326>

Received 23 September 2023; Received in revised form 21 January 2024; Accepted 28 January 2024

Available online 8 February 2024

0360-3199/© 2024 The Authors. Published by Elsevier Ltd on behalf of Hydrogen Energy Publications LLC. This is an open access article under the CC BY license (<http://creativecommons.org/licenses/by/4.0/>).

**Nomenclature**

ANN	Artificial neural network
CART	Classification and regression tree
CGE	Cold gas efficiency
FC	Fixed carbon
GBR	Gradient boosting regression
GI	Gini index
GP	Gaussian process
HC	Light hydrocarbons
HHV	Higher heating value (MJ/kg)
HTS	High-temperature shift
KNN	K-nearest neighbour
LHV	lower heating value (MJ/kg)
LTS	Low-temperature shift
ML	Machine learning

np	Numpy
NRMSE	Normalized root mean square error
pd	Pandas
PET	Polyethylene terephthalate
PSA	Pressure swing adsorption
PS	Polystyrene
PP	Polypropylene
QET	Quasi-equilibrium temperature
R <sup>2</sup>	Regression co-efficient
RF	Random Forest
RSM	Response surface methodology
SVM	Support vector machine
SVR	Support vector regression
VM	Volatile matter
WGS	Water gas shift

approximately 70 %, is expected to be deposited in landfills that have limited potential for recycling [8]. Typical methods like burning are insufficient in addressing the disposal needs of waste plastics due to their technical limitations [9].

Polystyrene (PS) and PS-based plastics, despite their widespread usage, around 9 % in the European Union, have a 0.9 % recycling rate and recycling these specific types of plastics through the mechanical process would cause the polymer characteristics to deteriorate throughout the reprocessing, leading to a decrease in the overall quality of the recycled products [10,11]. Polypropylene (PP) significantly contributes to the plastic waste crisis, accounting for 29.6 % of all plastic waste demand [12]. Additionally, the recycling rate for PP is a mere 0.6 %, highlighting the potential environmental hazards associated with this material [10].

Thermochemical conversion of plastics emerges as a promising method for recycling plastics and waste management due to their high carbon (C) content and significant calorific value. Furthermore, the method offers the potential to recover heat and produce electricity using an internal combustion engine (ICE), making it suitable for decentralized power generation [13]. The three primary forms of thermochemical conversion encompass combustion, pyrolysis, and gasification [14]. The pyrolysis process of plastic has the potential to generate oil, char, and gas, while plastic gasification mainly yields syngas rich in H<sub>2</sub> [15,16]. Previous studies have demonstrated that the co-pyrolysis of PP and PS exhibits a thermal cracking enhancement effect, resulting in synergistic improvements in the production yields of H<sub>2</sub>, light hydrocarbons (HC), and overall syngas compared to their pyrolysis processes [17,18]. Gasification is noteworthy as it converts plastic waste into synthetic gas, a potential energy source, thereby demonstrating a commitment to sustainability. Additionally, gasification diminishes dependence on traditional waste disposal methods, steering nations closer to a circular economy [19]. Moreover, as fossil fuels diminish and their environmental consequences become more evident, there is a growing imperative to explore substitute energy sources like hydrogen. This element is highly valued for its environmentally friendly combustion process. Additionally, hydrogen derived from the gasification of plastics and biomass possesses a lower heating value. Its combustion results in the production of only water, rendering it a versatile and economically efficient fuel [20]. Numerous articles have emphasized the economic benefits of utilizing fluidized bed gasification in the thermochemical conversion of waste. Studies have confirmed its economic feasibility even when considering dual fluidized bed gasification. These results imply that fluidized bed gasification technologies present promising economic opportunities for hydrogen production [21]. In fluidized bed gasification systems, a bed material is employed to facilitate the fluidization of biomass within the reactor. The augmentation of fluidization

enhances the homogeneous distribution of materials and heat, and improves reaction efficiency. Compared to fixed-bed and plasma gasification systems, fluidized bed gasification stands out with its high efficiency, uniform temperature distribution, and economic advantages [22,23].

Syngas, composed primarily of H<sub>2</sub>, CO, CH<sub>4</sub>, and CO<sub>2</sub>, demonstrates a robust association between its yield and composition and multiple operational variables. These factors encompass the characteristics of the feedstock, the composition and ratio of feedstock employed, reaction temperature, and the specific gasifying agent utilized [18]. Notably, H<sub>2</sub> possesses dual significance as a high energy carrier and a vital feedstock within the chemical industry. Its versatile applications include the synthesis of valuable products through hydrogenation and hydrotreatment processes, contributing to its pivotal role in various industrial contexts [9]. In the past few years, numerous investigations have been undertaken to anticipate the optimal operational parameters and performance of systems, relying on diverse gasification agents including air [24,25], pure steam [26–28], mixtures of air and steam [29,30], oxygen and steam [31], and carbon dioxide [18].

In recent studies, the main focus has been directed towards the thermomechanical conversion of biomass or mixed plastics and biomass when employed as a feedstock [32,33]. For instance, in gasification of mixed rice husk and groundnut shell and palm oil decanter cake and alum sludge, reducing feedstock sizes enhances specific surface area, thereby promoting higher rates of heating and gasification, ultimately leading to increased yields of H<sub>2</sub> and improved efficiencies in carbon conversion [34,35]. Zallaya et al. [36] have demonstrated that elevating the gasification temperature during steam gasification of polyethylene (PE) and polyethylene terephthalate (PET) leads to a reduction in H<sub>2</sub> content and an increased presence of CH<sub>4</sub> in the resulting gas phase. Yang et al. [37] compared the performance of ANN, SVM and MLR using 1855 data points, on coal and biomass gasification, highlighting the accuracy of ANN and SVM compared to MLR.

In a comparative study conducted by Mojaver et al. [38], it was noted that biomass gasification leads to greater CO<sub>2</sub> emissions in comparison with different plastic materials. The co-utilization of plastic and biomass presents plausible environmental risks. However, it's crucial to emphasize that the use of biomass is constrained, especially in terms of land availability [39]. Moreover, the existing research concerning the pyrolysis and co-gasification of PS and PP plastics is limited, particularly in terms of investigating the ideal operating conditions for generating hydrogen-rich syngas. The efficacy of the gasification process is mainly influenced by a range of process parameters, including the type of biomass, flow rate of the gasifying agent, elemental composition of the biomass, configuration of the gasifier, nature of the gasifying agent, operating temperature, pressure, and the ratio of fuel to feedstock [40].

Machine learning (ML) has become increasingly popular due to its effectiveness in handling huge quantities of data and facilitating predictions and optimization [41]. The adoption of ML has garnered considerable recognition for its significant benefits in the area of data analysis, enabling the optimization of thermomechanical conversion processes for various materials while uncovering complicated data patterns rather than conventional time-consuming techniques and empirical approaches [42–44]. Furthermore, conventional methods of optimization face the ongoing challenge of accurately predicting system performance when multiple operating parameters vary simultaneously, and they struggle to forecast gas product distribution and process performance during the blending of two distinct feedstocks [45]. A significant portion of the recent scientific investigations associated with the utilization of ML techniques in thermomechanical conversion processes has primarily focused on the optimization of biomass gasification or pyrolysis [37,46–48]. Kim et al. [49] utilized ML techniques, specifically Random Forest (RF), Artificial Neural Network (ANN) and Support Vector Machine (SVM) using 484 data points, to forecast the production of syngas in fluidized bed reactors, focusing on the utilization of wood and agricultural residue as combined feedstock. ANN and RF exhibited a remarkable level of accuracy in their individual investigations compared to SVM, shedding light on crucial variables within the gasification process. Fang et al. [50] utilized Monte Carlo approach and RF for optimizing fixed bed air gasification with wood as a feedstock. The RF model indicated a significant impact of particle size, reaction temperature, and water content on the syngas yield. Likewise, better performance by ANN has been demonstrated by the study conducted by Hai et al. [51] on optimization of biomass gasification for electricity generation to predict optimal process condition compared to SVM.

Despite the potential benefits that can arise from this approach, a limited number of scholarly investigations have examined the critical parameters and optimization techniques related to the thermochemical conversion of plastic using ML methods. Mojaver et al. [52] undertook an investigation focusing on the enhancement of gasification processes for polypropylene, polyethylene, polycarbonate, and polyethylene terephthalate (PET) plastics using the Taguchi method. The findings indicated that the steam-to-plastic fraction, the temperature of gasification, and the type of plastic are significant factors influencing the production of hydrogen-rich syngas. Moreover, the study highlights a notable decrease in CO<sub>2</sub> generation with increasing gasification temperature. Ayodele et al. [53] investigate ML modelling for the co-gasification of rubber and plastics with the objective of predicting the H<sub>2</sub> percentage in syngas. The study achieved a remarkably high prediction accuracy of 0.99 by including four specific conditions as input variables. In the investigation of pyrolysis oil yield from different types of plastic, Cheng et al. [54] utilized ANN, Gaussian Process (GP), and Support Vector Machine (SVM) methodologies. The results indicated that among these models, ANN and SVM demonstrated superior performance with R-squared values of 0.98 and 0.92, respectively. The operating temperature and residence time have been also mentioned as key operating parameters.

These studies lacked comprehensive findings regarding the co-gasification of PP and PS plastics, as well as a comprehensive assessment of how the operating conditions influence the outcomes of the process. Response surface methodology (RSM) has been used to optimize microwave-assisted co-pyrolysis of PS and PP plastics with a high accuracy of 0.99 by Kamireddi et al. [17]. Hence, a lack of reliable information exists regarding the precise optimization approach for the pyrolysis and co-gasification of plastics. Consequently, Additional investigation is essential to assess the effectiveness of various ML models in the co-pyrolysis and co-gasification of PP and PS plastics. The determination of operational parameters plays a pivotal role in attaining the highest H<sub>2</sub> Production. Nonetheless, this task poses a significant challenge owing to the nonlinear characteristics of the process, making it difficult to accomplish using conventional approaches. Hasanzadeh et al. [55] enhance the gasification of PE plastic using RSM. The results

have shown the RSM accuracy in predicting the syngas yield with RMSE smaller than 1. In this investigation, the foremost intention is to design a comprehensive steady state model utilizing the ASPEN Plus V12.1 simulation program. The model is designed to depict the pyrolysis and steam co-gasification processes of two plastics, namely PP and PS, in a ratio of 2:3 (40 % PP and 60 % PS). The highest level of cooperative enhancement in H<sub>2</sub> generation was observed when co-gasification blends of PP and PS containing 40 % PP composition [18]. This process holds a significant promise for both waste plastic management and the generation of hydrogen-rich syngas. Through sensitivity analysis, the study examined the effects of operational variables, encompassing the temperature and pressure within the gasification unit, and the flow rate of steam, which influenced the composition of the generated syngas. This research also developed inclusive ML models that effectively optimize the co-gasification processes of PS and PP plastics. The dataset employed in this study has been obtained from the Aspen. Furthermore, the analysis has been conducted on various models used by previous studies to identify the most optimal model capable of clarifying the influence of input factors on the process's overall outcome.

## 2. Machine learning models

### 2.1. Random Forest (RF)

RF utilizes a collection of decision trees, making it applicable for both regression and classification tasks [56,57]. This approach involves generating multiple subsamples from a dataset consisting of  $n$  input variables and  $m$  associated features, and each tree in the RF is trained on one of these subsamples [49]. The subsamples are further divided into in-bag and out-of-bag data, with a ratio of 0.67:0.33 [58,59]. Out-of-bag data is used as an expansion of the decision tree without a pruning approach, while in-bag data has been used for the regression model [56]. The RF method also employs a preventive approach against overfitting compared to individual decision trees through the implementation of bagging techniques, while achieving this by training multiple decision trees on randomly selected subsamples from the training data (bagging techniques) and having limited tree depth [60].

### 2.2. Artificial Neural Network (ANN)

ANN is a computational model inspired by the human brain. It finds widespread application in various domains, including signal processing, and simulating processes [47]. ANN typically comprise a minimum of three layers and the initial layer establishes a connection with the input dataset, while subsequent layers are obtained through the process of multiplying a weight matrix and incorporating a bias term [61]. Various activation functions are then employed to iteratively adjust the weight and bias to reduce the sum square difference (error) between the predicted model and real data observed from a known set of training data [49]. In the context of thermochemical conversion where the relationship among input parameters, such as reactor temperature and pressure, and process output is quite intricate, ANN can effectively model the process since it does not require to understand the underlying mechanism [62]. The model in this investigation consists of a single hidden layer with ten neurons, while the input layer has a dimension of three, corresponding to the number of variables.

### 2.3. Gradient Boosting Regression (GBR)

GBR has been traditionally found beneficial in classification tasks, yet its efficacy in regression analysis has attracted significant attention because of its exceptional precision [63,64]. It employs a boosting strategy in combination with gradient descent to train the datasets, and the initial GBR model is optimized by following the negative gradient direction of the primary model [65]. Then, the tree is developed in each step using an average of output values as an input to calculate the error

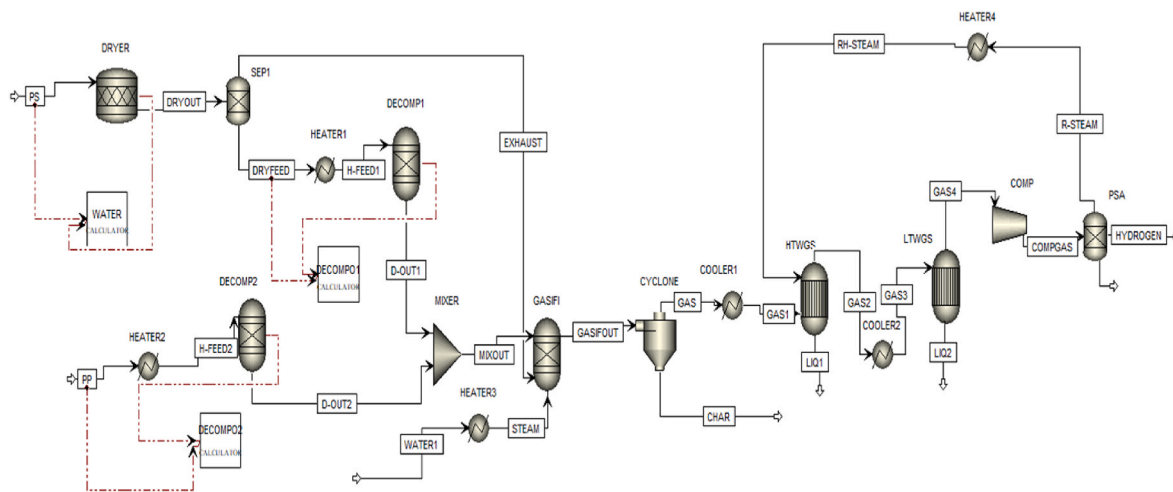


Fig. 1. Aspen plus flowsheet evaluated in this study.

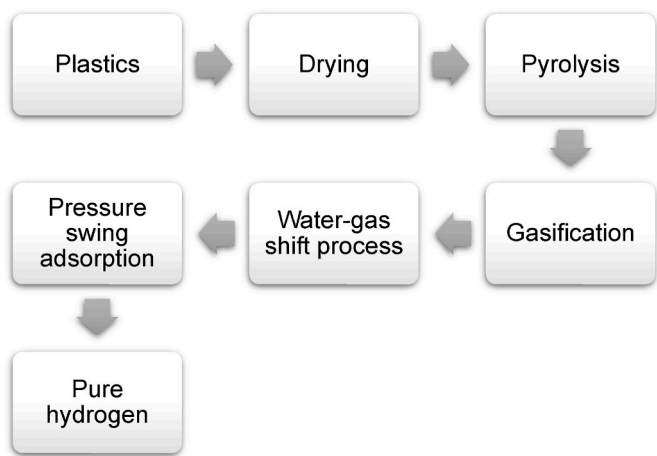


Fig. 2. The diagram illustrating the process of plastic gasification for hydrogen production.

of the tree and the process continues until there is no considerable residue [66]. Like RF, GBR is a tree-based approach to fit the data for regression techniques, and the number of decision trees and maximum depth are crucial factors [67].

2.4. Classification and Regression Tree (CART)

CART algorithm represents a combined approach of the classification decision and regression tree algorithms [68]. The algorithm partitions the original dataset into two distinct subsets by utilizing either the Gini index (GI) or the towing indices, and these indices serve as indicators of the impurity level present within the data [69]. The smaller value of GI demonstrates the high purity of nodes, and the process stops when reaching a specific tree depth, minimum number of data points in a node, and high level of purity [70].

2.5. K-nearest neighbour (KNN)

KNN algorithm is a known technique in the field of ML. It possesses several notable strengths, including its ability to deliver accurate predictions, robustness against outliers, and efficient training speed [71]. This approach is based on the nearest neighbour and the distance which can be determined by the below criteria [72].

$$\text{Euclidean distance} = \sqrt{\sum_{i=1}^k (y_i^{exp} - y_i^{pred})^2} \tag{1}$$

$$\text{Manhattan distance} = \sum_{i=1}^k |y_i^{exp} - y_i^{pred}| \tag{2}$$

$$\text{Minkowski distance} = \left( \sum_{i=1}^k (|y_i^{exp} - y_i^{pred}|)^q \right)^{\frac{1}{q}} \tag{3}$$

By utilizing the distances of the k nearest samples to the target sample and computing their weighted average, it becomes possible to figure out the estimated value of the sample, which can then be employed in determining the ultimate prediction value [73].

2.6. Support Vector Regression (SVR)

SVR is an enhanced algorithm derived from the Support Vector Machine (SVM) framework, specifically designed to address regression tasks with a powerful binary classification model that operates as a linear classifier, distinguishing between two classes by maximizing the margin in the feature space [74]. It employs the nonpragmatic regression model to ascertain the distance to the adjacent data points, commonly referred to as support vectors [75]. To address the challenges posed by non-linearly separable problems, SVR employs the utilization of kernel function pairs to facilitate the mapping of samples from lower latitudes to higher latitudes [74]. This approach enables SVR to effectively handle complex data distributions that do not exhibit linear separability. The kernel functions ‘rbf’, ‘linear’, and ‘poly’ are frequently employed in various computational tasks [75].

3. Methodology

3.1. Process simulation

The plastics gasification system was represented in a flowsheet, as depicted in Fig. 1. The initial stage of the gasification procedure, involving drying and pyrolysis, was simulated. To enhance H<sub>2</sub> yield and reduce CO concentration, two WGS units were implemented. Furthermore, the separation unit block was examined, initially focusing on the PSA unit. Fig. 2 represents the schematic of the plastic gasification system.

The gasification process was modelled with the following assumptions, which were taken into consideration:

**Table 1**  
The list of components.

Component ID	Type	Component Name
H <sub>2</sub>	Conventional	Hydrogen
N <sub>2</sub>	Conventional	Nitrogen
O <sub>2</sub>	Conventional	Oxygen
CH <sub>4</sub>	Conventional	Methane
CO <sub>2</sub>	Conventional	Carbon dioxide
C	Solid	Carbon-Graphite
H <sub>2</sub> O	Conventional	Water
CO	Conventional	Carbon monoxide
S	Conventional	Sulfur
Polypropylene (PP)	Non-conventional	–
Polystyrene (PS)	Non-conventional	–
Ash	Non-conventional	–

- The process operates under steady-state conditions and isothermal.
- Drying and pyrolysis reactions occur immediately, resulting in volatile products primarily composed of H<sub>2</sub>, CO<sub>2</sub>, CH<sub>4</sub>, CO, and H<sub>2</sub>O.
- The char produced includes only carbon and ash.
- All gases involved in the process exhibit ideal behaviour.
- Negligible tar formation attributed to operating at elevated temperatures.

Table 1 presents a comprehensive inventory of components employed in the simulation model. The characterization of plastics is achieved through both ultimate and proximate analyses, and plastics are categorized as nonconventional elements. Detailed specifications of the feedstock utilized are documented in Table 2. The HCOALGEN and DCOALIGT models play a crucial role as they are utilized to precisely determine not only the enthalpy but also the density of plastics and ash. The Peng-Robinson equation of state with Boston- Mathias (PR-BM) modification due to accuracy in high-temperature processes including gasification is used to determine the thermodynamic characteristics of the conventional material in Aspen Plus.

To simulate the drying process of PS plastic and reduce the moisture content, the RSTOIC reactor model is employed. Control over the drying operation is established by incorporating a FORTRAN statement within the calculator block. After the drying process, the moisture content is removed and isolated through a separation step using a separator. The resulting dried plastic is then subjected to preheating at a temperature of 700 °C via a heater block. The other stream (PP) undergoes direct preheating to the same temperature using a separate heater block. It is worth noting that Thermal degradation of PP and PS plastics occur between 563 °C and 763 °C [18]. In the subsequent step, two RYIELD reactors are employed to facilitate the pyrolysis of the dried plastics into its constituent components, leading to the formation of primary outputs such as H<sub>2</sub>O, H<sub>2</sub>, C, O<sub>2</sub>, N<sub>2</sub>, S, and ash. The FORTRAN instruction is specifically designed to define the distribution of yield for plastics into the resulting products [78].

Following the pyrolysis process, the resulting streams are combined to form the feed for the gasifier. Subsequently, the stream containing the pyrolysis products undergoes a conversion process within an RGIBBS (GASIFI) reactor, where the components are transformed into a mixture of gas and solid utilizing a gasification agent, namely steam. The gasifier was simulated using the quasi-equilibrium temperature (QET) approach,

**Table 2**  
The proximate and ultimate analyses conducted on the feedstocks employed in this investigation.

Plastic	Proximate content				Ultimate Analysis					HHV <sup>c</sup> (MJ/kg)	Ref
	VM <sup>a</sup>	FC <sup>b</sup>	ASH	Moisture	H	N	C	S	O		
PP	96.48	2.63	0.89	0	13.99	0.09	85.03	–	–	46.79	[76]
PS	98.31	0.8	0.1	0.79	5.74	–	93.76	–	0.5	41.1	[77]

<sup>a</sup> Volatile matter.

<sup>b</sup> Fixed carbon.

<sup>c</sup> Higher heating value.

which is a highly effective method for modelling fluidized-bed gasification. This approach offers a precise characterization of the syngas composition [1]. The reactions taking place inside the gasification reactor, as detailed in Table 3, are carried out at their corresponding QET values, not at the reactor's real temperature. A CYCLONE unit separates the gas products from the char in the subsequent stage. Table 4 provides a summary of the blocks utilized within this simulation study.

The syngas generated from the gasifier is subjected to the water-gas shift reaction, denoted as Reaction R<sub>5</sub>. This reaction occurs in two distinct reactors: the high-temperature shift (HTS) reactor and the low-temperature shift (LTS) reactor. The utilization of these two reactors stems from the fact that the water-gas shift reaction is moderately exothermic. In accordance with Le Chatelier's principle, when temperatures are increased, the reaction tends to favour the reverse direction, impeding full conversion. While the HTWGS reactor facilitates the initial conversion of CO due to its fast kinetics, it still falls short of surpassing the equilibrium point. Therefore, the LTWGS reactor becomes crucial for achieving additional conversion [1,29].

The gas exiting these two reactors primarily consists of H<sub>2</sub>, CO<sub>2</sub>, N<sub>2</sub>, and small quantities of CH<sub>4</sub>, CO, and O<sub>2</sub>. To obtain pure H<sub>2</sub>, it becomes necessary to separate these gases. Therefore, the gas stream following the WGS reactors is directed into a PSA system to achieve the desired purification and obtain pure H<sub>2</sub>. The H<sub>2</sub> yield is determined using the following equation [84]:

$$\text{Hydrogen yield} = \frac{\text{Hydrogen mass flow in gasifier reactor output} \left( \frac{\text{kg}}{\text{h}} \right)}{\text{Feedstock mass flow (dry basis)} \left( \frac{\text{kg}}{\text{h}} \right)} \quad (4)$$

### 3.2. Performance parameter

Cold gas efficiency (CGE) stands as a key metric for assessing the gasifier's effectiveness in adapting to alterations in the operational parameters of the gasification process [85]. It is calculated by determining

**Table 3**  
Primary heterogeneous and homogeneous gasification reactions [79–84].

Reaction No.	Reaction	Reaction name	Heat of reaction (MJ kmol <sup>-1</sup> )
R <sub>1</sub>	C + O <sub>2</sub> → CO <sub>2</sub>	Carbon total combustion	–394
R <sub>2</sub>	C + 0.5 O <sub>2</sub> → CO	Carbon partial combustion	–111
R <sub>3</sub>	CO + 0.5 O <sub>2</sub> → CO <sub>2</sub>	Carbon monoxide partial combustion	–283
R <sub>4</sub>	C + H <sub>2</sub> O ⇌ CO + H <sub>2</sub>	Water-gas	131
R <sub>5</sub>	CO + H <sub>2</sub> O ⇌ CO <sub>2</sub> + H <sub>2</sub>	Water-gas shift	–41.2
R <sub>6</sub>	C + CO <sub>2</sub> ⇌ 2CO	Boudouard	172
R <sub>7</sub>	C + 2H <sub>2</sub> ⇌ CH <sub>4</sub>	Hydrogasification	–74.8
R <sub>8</sub>	CO + 3H <sub>2</sub> ⇌ CH <sub>4</sub> + H <sub>2</sub> O	Methanation	–206
Pyrolysis R <sub>9</sub>	Dry feedstock + Heat → Char + Volatiles	Thermal decomposition	NA <sup>a</sup>

NA<sup>a</sup> = Not Available.

**Table 4**  
ASPEN Plus flowsheet unit operations description in the developed model.

Aspen plus name	Block ID	Description
RGibbs	GASIFI	Gibb’s free energy reactor - controls chemical equilibrium of the main reactions (Temperature = 900 °C; Pressure = 1 bar)
Rstoic	DRYER	Depletes the moisture content of plastic (PS) through a drying process (Heat Duty = 0 kJ/h; Pressure = 1 bar)
Sep	SEP1	Extracts water from plastic (PS) through separation
PSA	PSA	Obtains pure H <sub>2</sub> through extraction
Heater	HEATER1	Raises the temperature of the dried plastic (PS) to meet the required temperature in the pyrolysis reactor (Temperature = 700 °C; Pressure = 1 bar)
	HEATER2	Increases the temperature of the plastic (PP) to meet the required temperature in the pyrolysis reactor (Temperature = 700 °C; Pressure = 1 bar)
	HEATER3	Elevates the temperature of water to achieve the steam phase
	HEATER4	Brings the temperature of the recycle steam to the required temperature in the HTWGS reactor
COOLER1	COOLER1	Lowers the temperature of syngas to the prescribed level in the HTWGS reactor (Temperature = 400 °C)
	COOLER2	Decreases the temperature between HTWGS and LTWGS
RYield	DECOMP1	Converts the non-conventional stream (PS) into its conventional components (Heat Duty = 0 kJ/h; Pressure = 1 bar)
	DECOMP2	Converts the non-conventional stream (PP) into its conventional components (Heat Duty = 0 kJ/h; Pressure = 1 bar)
Mixer	MIXER	Mixes the pyrolysis products
Cyclone	CYCLONE	Separates the products of gasification
REquil	HTWGS	Simulates the water-gas shift reaction under high-temperature conditions
	LTWGS	Simulates the water-gas shift reaction under low-temperature conditions
Compr	COMP	Increases the gas pressure preceding the PSA process

the ratio of syngas energy to feedstock energy as shown in Eq. (5):

$$CGE = \frac{M_{\text{syngas}} \times LHV_{\text{SYNGAS}}}{M_{\text{Feedstock}} \times LHV_{\text{Feedstock}}} \quad (5)$$

where M represents the mass flow rate, and LHV signifies the lower heating value. The Lower Heating Value (LHV) of the feedstock is obtained from prior studies conducted by Li et al. [18]. The LHV of syngas signifies the energy released during the complete oxidation of syngas,

omitting the heat related to water vaporization in combustion products. This specific value for the LHV of syngas can be accessed in the stream characteristics section of Aspen PLUS.

### 3.3. Machine learning methodology

The field of ML encompasses a diverse array of algorithmic approaches, which can be broadly classified into four distinct categories including supervised, semi-supervised, unsupervised, and reinforced learning [66,86]. Supervised learning is an approach to ML in which a model is trained to learn the mapping between input data and the associated outputs. This is achieved by providing the model with input-output pairs, which it uses to iteratively adjust its internal parameters and improves its ability to accurately predict outputs for new inputs [86]. Despite the numerous advantages of machine learning-driven models, a dearth of comparative analysis persists regarding H<sub>2</sub> production from PP and PS plastics. Fig. 3 illustrates a systematic machine learning-driven approach aimed at optimizing the co-gasification of two plastic materials through the utilization of multiple techniques.

### 3.4. Data preparation and dataset compiling

Previous researchers have identified gasification reactor temperature, pressure, and mass flow rate of the gasifying agent as the key variables that have an important influence on the process product [52, 87]. In this investigation, the Python programming language has been employed to utilize the numpy (np), pandas (pd), and sklearn

**Table 5**  
Model validation.

Plastics	Literature data (vol %)		This study (vol %)		Relative error <sup>a</sup>	
	H <sub>2</sub>	CO	H <sub>2</sub>	CO	H <sub>2</sub>	CO
1P4S	16	82	17	77	6.25	6.1
2P3S	19	79	20	73.7	5.26	6.7
3P2S	19	76	22.8	70.5	20	7.2
4P1S	20	72	25.4	67.5	27	6.25
PP	21	66	27.8	64.7	32.4	1.96
PS	15	82	15.3	82.5	2	0.97

<sup>a</sup> RE = Relative error =  $\frac{|(\text{Simulation value} - \text{Experimental value})|}{\text{experimental value}}$

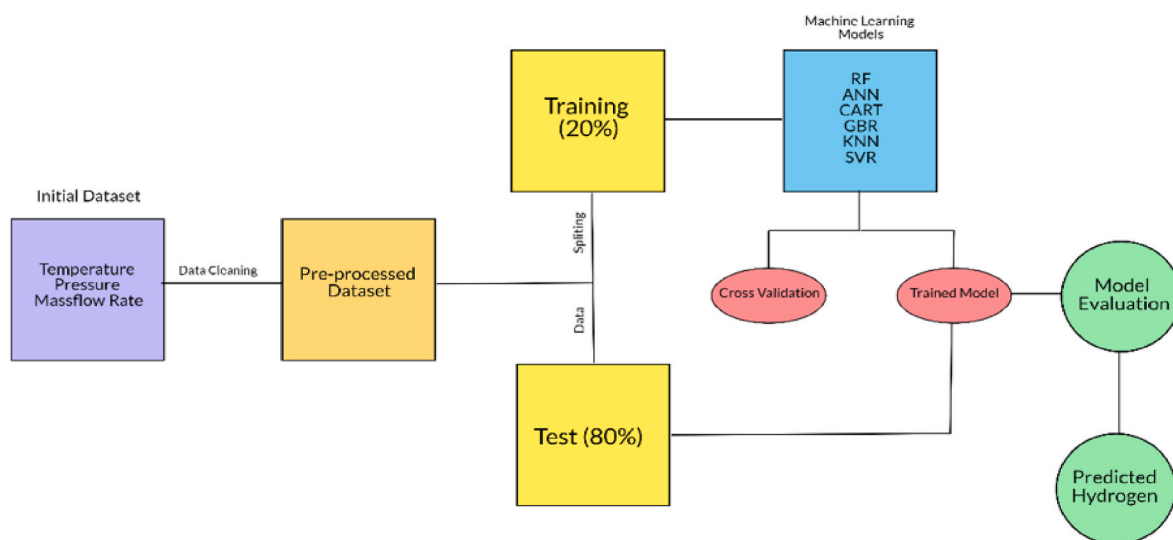


**Fig. 3.** ML-based systematic strategy for optimizing co-gasification of two plastics using various techniques, including Neural Networks, Support Vector Regression, Random Forest, Gradient Boosting Regression, Classification and Regression Tree, and K-Nearest Neighbours.

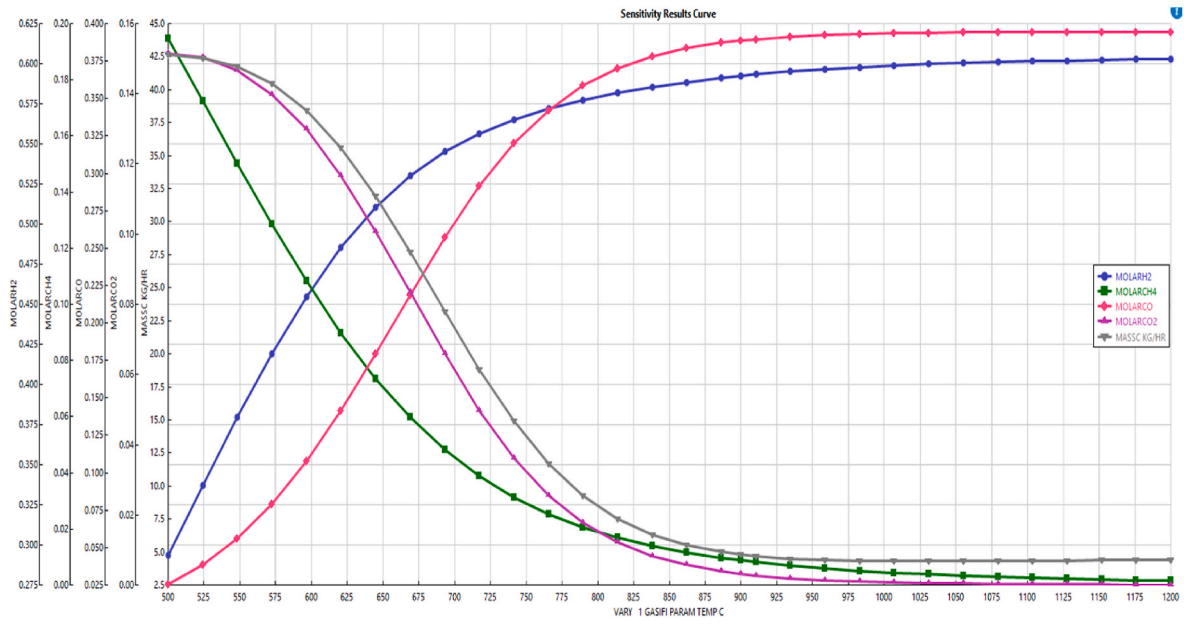


Fig. 4. The impact of gasification temperature on the syngas composition exiting the gasifier.

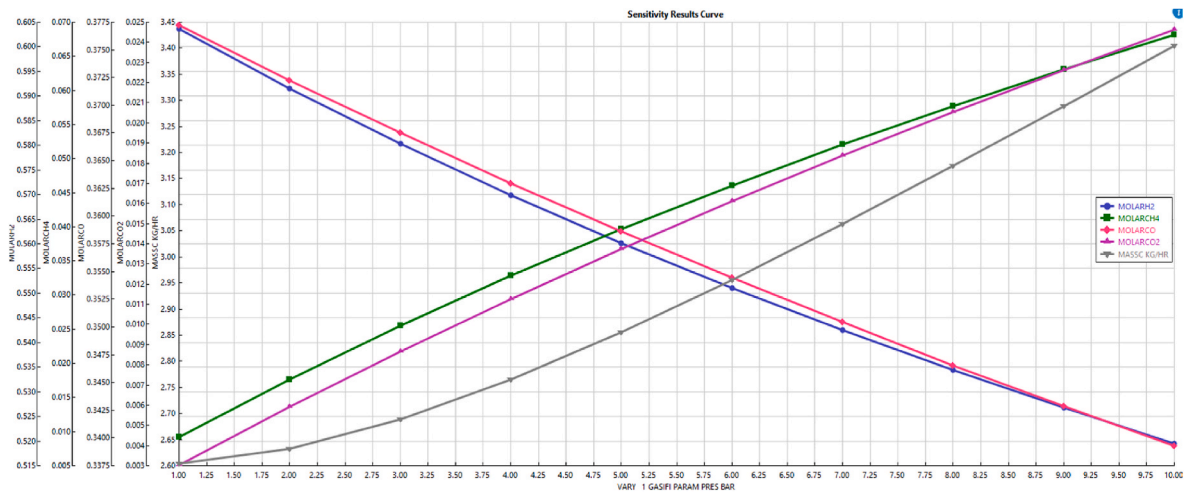


Fig. 5. The impact of gasification pressure on the syngas composition exiting the gasifier.

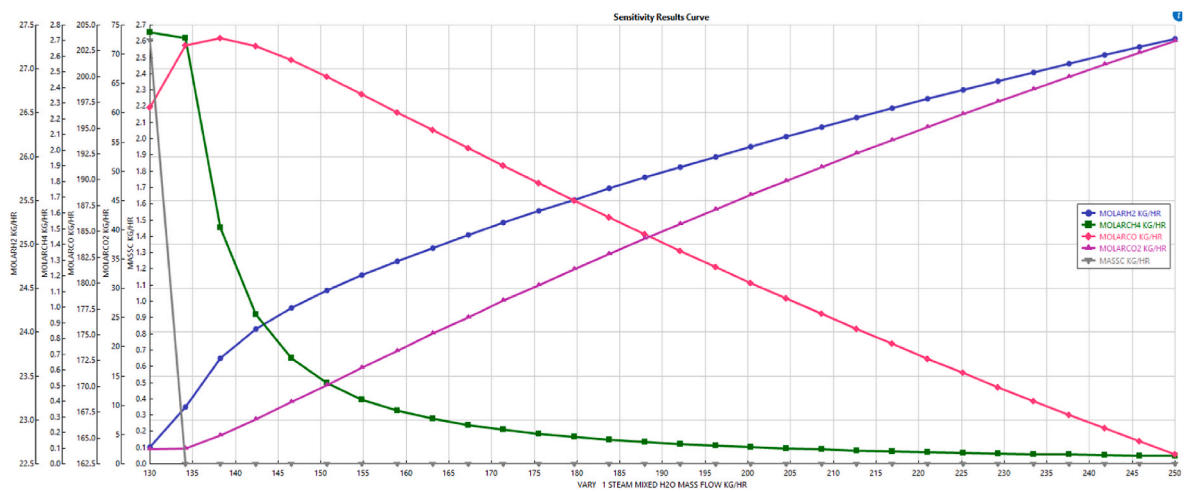


Fig. 6. The impact of gasifying agent mass flowrate on the syngas mass flowrate exiting the gasifier.

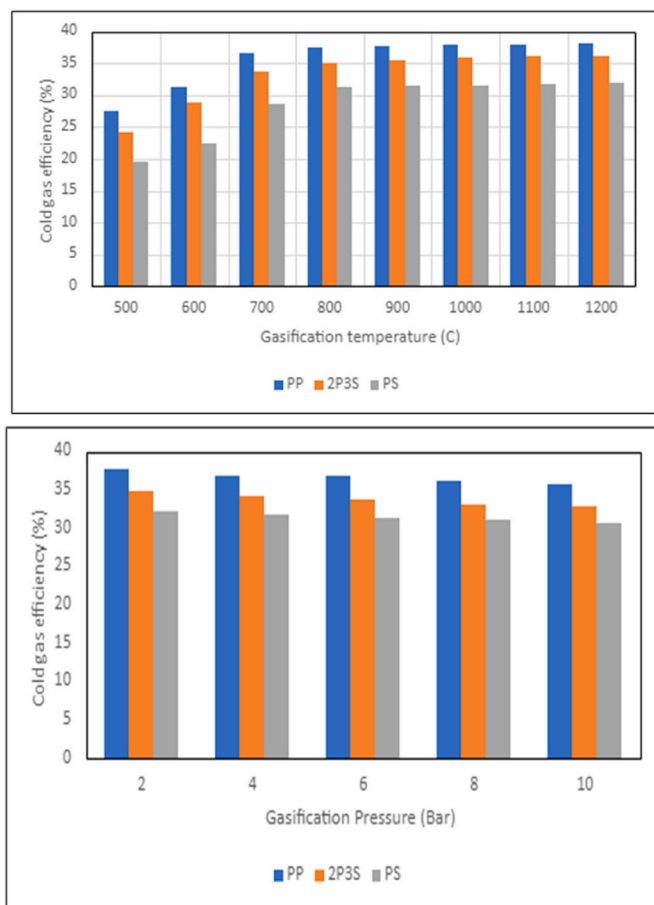


Fig. 7. The impact of temperature and pressure on cold gas efficiency.

**Table 6**  
ML Models Comparison and Prediction Performance (training data).

Model	R <sup>2</sup>	NRSME
RF	0.9996	0.0054
ANN	0.9917	0.0263
GBR	0.9963	0.0176
CART	0.9985	0.0112
KNN	0.9985	0.0111
SVR	0.9977	0.0139

(scikit-learn) libraries. These libraries have been leveraged to develop and implement ML methodologies. To ensure a rigorous evaluation, the dataset, with 9000 datasets, is divided into two distinct training and test sets which is a common approach for ML model developments. The datasets were created using Aspen Plus, with a specific focus on the sensitivity analysis section, emphasizing key parameters. The chosen input variables include temperature, pressure, and steam mass flow rate, while the output data comprises molar fractions of H<sub>2</sub>, CH<sub>4</sub>, CO<sub>2</sub>, and CO. Specifically, 80 % of the dataset has been allocated for training the model, while the remaining 20 % of the dataset has been utilized as a test to generate syngas yield predictions. To address the issue of overfitting arising from a limited dataset, this study employs a 10-fold cross-validation technique to determine the most suitable hyperparameters for the test model [88,89]. In detail, the training set is partitioned into ten distinct folds, with nine of these folds acting as a new training set while the remaining fold is dedicated to validating the data. Following the completion of 10 training iterations, each fold underwent training and subsequently received evaluation using a set of predefined evaluation indicators. Subsequently, the hyperparameters are

determined based on the mean values of the evaluation metrics obtained from the ten iterations. The best hyperparameter configuration is utilized on the complete training dataset, and subsequently, the trained model is assessed and tested on the dedicated test dataset. Two evaluation indicators, Regression Co-efficient (R<sup>2</sup>) and Normalized-Root-Mean-Square Error (NRMSE) employed in this paper as evaluation indicators, with the objective of discerning the model that exhibits the greatest degree of accuracy in its predictions [66,90].

$$R^2 = 1 - \frac{\sum_{i=1}^N (y_i^{exp} - y_i^{pred})^2}{\sum_{i=1}^N (y_i^{exp} - Y)^2} \quad (6)$$

$$NRMSE = \sqrt{\frac{\sum_{i=1}^N (y_i^{exp} - y_i^{pred})^2}{N}} / Y \quad (7)$$

While  $y_i^{exp}$  and  $y_i^{pred}$  are the actual and predicted values, Y represents the mean of the actual values, and N is the number of samples. A higher value of R<sup>2</sup> indicates a stronger degree of accuracy in the model's ability to predict data points [91]. NRMSE is an additional metric employed in combination with R<sup>2</sup> to elucidate the average percentage deviation between observed values and predictions and low values close to zero indicates high degree of precision in model prediction [92].

## 4. Results and discussions

### 4.1. Simulation model validation

The simulated model using Aspen Plus software was validated and evaluated by comparing it with experimental results reported by Li et al. [18]. They analysed the co-pyrolysis and CO<sub>2</sub> assisted co-gasification of PP-PS blends at a temperature of 900 °C using a fixed-bed reactor, well-suited for handling solid feedstocks, and its configurations provide a consistent environment for reactions. In order to validate the model, the simulation was performed under the same conditions as the experimental data. It is important to note that while steam was just used as a gasifying agent in this study, CO<sub>2</sub> was employed as supply gas in the gasifier reactor to align with the methodology used in the referenced article for validation. Four distinct polypropylene-polystyrene blends were employed in the study, characterized by varying PP contents of 20 %, 40 %, 60 %, and 80 %. These blends were denoted as 1P4S, 2P3S, 3P2S, and 4P1S, respectively.

Table 5 illustrates the gas composition of the syngas generated through the co-gasification of two mixed plastics with varying ratios. It is clear that the model results closely align with the experimental findings for PP and PS. The variance between the results obtained from Aspen Plus and the values found in the literature was quantified by determining the relative error in the composition of H<sub>2</sub> mol %, CO mol %. After analysing both the experimental data and the simulations, while taking into account the discrepancies noted in Tables 5 and it is evident that the model created in software is effective at predicting how plastics are converted. Specifically, the H<sub>2</sub> percentages range from 2 % to 32.4 %, and CO percentages is between 0.97 % and 7.2 %.

### 4.2. The effect of gasification temperature on the composition of syngas

Temperature plays a crucial role in gasification processes as it strongly influences the reaction rate. Higher temperatures effectively decompose plastics components, leading to increased syngas generation. Consequently, the production of syngas generally rises with temperature elevation. This can be attributed to the reactions mentioned in Table 3, which exhibit significant sensitivity to higher temperatures. Fig. 4 illustrates the relationship between the mole fraction of syngas generated by steam gasification of the blended plastics and the gasification temperature, ranging from 500 °C to 1200 °C. This finding is consistent with Le Chatelier's principle, which asserts that elevated temperatures

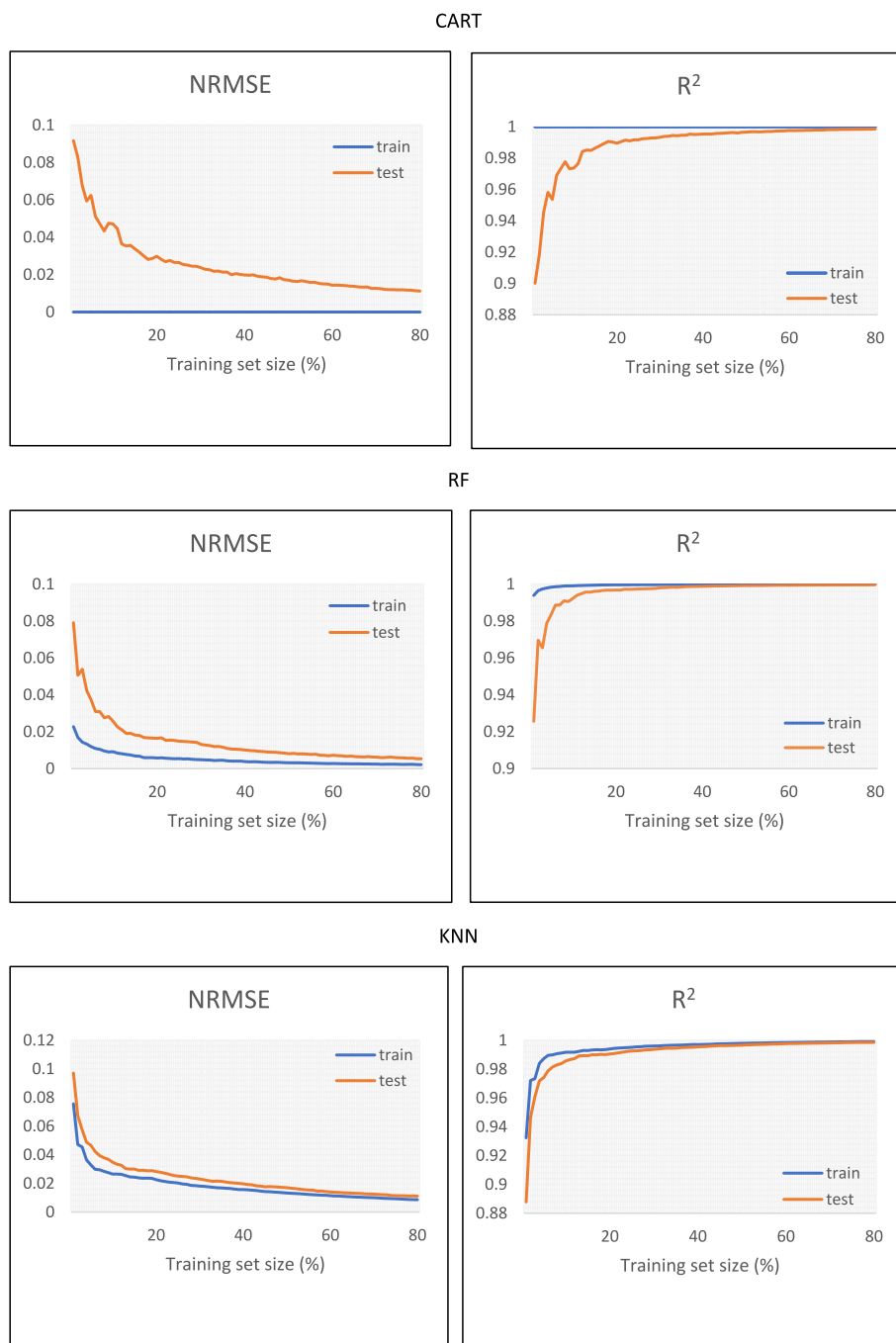


**Fig. 8.** Training and testing effectiveness of various machine learning algorithms in forecasting the mass flow rates of H<sub>2</sub>, CH<sub>4</sub>, CO<sub>2</sub>, and CO within syngas produced through gasification.

encourage the reactants, leading to increased conversion and a shift in the equilibrium towards the desired products [52,93]. At lower operating temperatures, the gasifier output contains both carbon, CH<sub>4</sub>, and CO<sub>2</sub>. As the temperature increases, carbon undergoes the endothermic Boudouard reaction (R<sub>6</sub>), converting it into CO. CH<sub>4</sub>, on the other hand, experiences exothermic reverse methanation (R<sub>8</sub>), transforming it into H<sub>2</sub>. Additionally, the temperature increase enhances H<sub>2</sub> and CO production while consuming more CH<sub>4</sub> and carbon, owing to the endothermic water-gas reaction (R<sub>4</sub>) and exothermic hydrogasification reaction (R<sub>7</sub>). It is worth noting that the H<sub>2</sub> yield intensifies from 6.87 % to 23.6 % when the temperature increases from 500 °C to 1200 °C. Overall, H<sub>2</sub> and CO production significantly increase with higher gasifier

temperatures. Notably, during steam gasification of blended plastics (2P3S), the mole fraction of H<sub>2</sub> and CO enhances from 0.299 to 0.6144 and 0.025 to 0.3827, respectively, as the temperature rises from 500 °C to 900 °C. However, beyond this, further temperature increases in the range of 900 °C–1200 °C do not lead to significant enhancement in production rates. Consequently, it can be assumed that using higher temperatures to generate more syngas above 900 °C is not economically favourable.

#### 4.3. The effect of gasification pressure on the composition of syngas

Gasifier pressure constitutes a significant operational parameter with

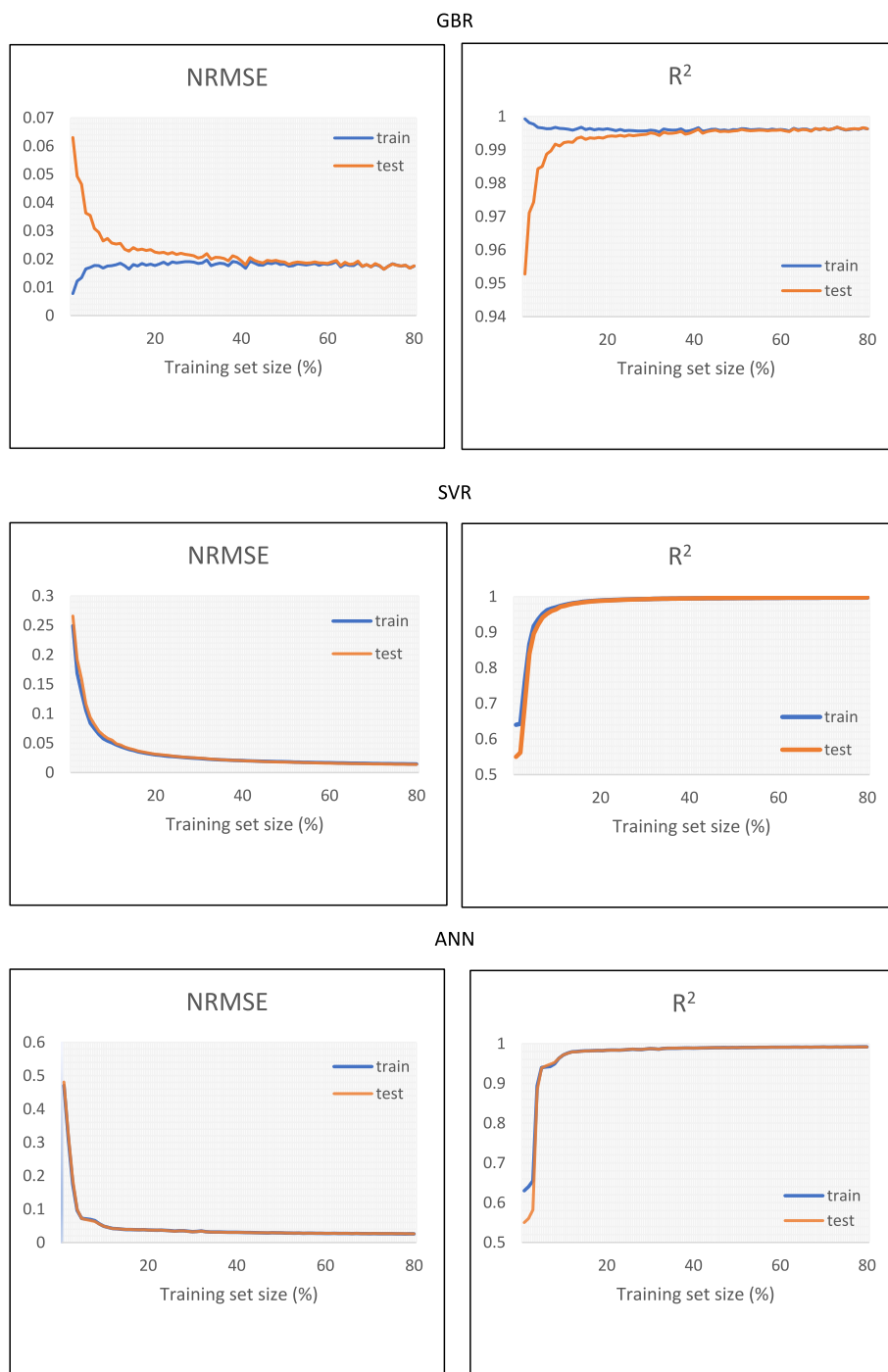


Fig. 8. (continued).

substantial implications for the performance of the gasification process. Increased pressure levels lead to improved process efficiencies, especially when considering subsequent operations that involve pressurized gas streams. According to Le Chatelier's principle, when pressure rises, the equilibrium shifts toward the side of the reaction with fewer gaseous moles, whereas a decrease in pressure encourages a shift toward the side with a higher number of gaseous moles [81].

The impact of gasifier pressure, ranging from 1 to 10 bar, on the mole fraction of syngas in the case of blended plastic is graphically depicted in Fig. 5. This pressure variation, in accordance with the primary gasification reactions (as outlined in Table 3), intensifies CO<sub>2</sub> and carbon production through the Boudouard (R<sub>6</sub>) and water-gas (R<sub>4</sub>) reactions.

Furthermore, hydrogasification (R<sub>7</sub>) and methanation (R<sub>8</sub>) reactions contribute to increased CH<sub>4</sub> production. It is evident from this illustration that H<sub>2</sub> yield diminishes as gasifier pressure increases, with a pressure of 1 bar yielding maximum H<sub>2</sub> production for all feed compositions. The H<sub>2</sub> yield experiences a reduction from 22.64 % to 17.4 % as pressure rises from 1 to 10 bar. Consequently, H<sub>2</sub> and CO gas production diminishes with increasing pressure from 1 to 10 bar, resulting in a decrease in the mole fraction of H<sub>2</sub> (from 0.6 to 0.52) and CO (from 0.38 to 0.34). Concurrently, larger quantities of CHAR, CH<sub>4</sub>, and CO<sub>2</sub> are generated, which are generally not regarded as desirable products within the gasification process.

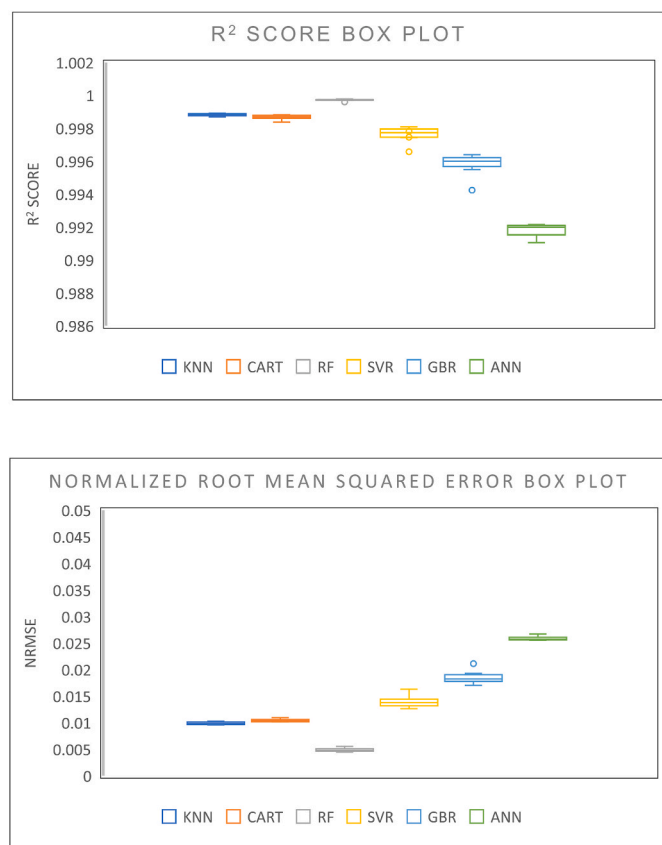


Fig. 9. Box plot performance of machine learning algorithms for predicting mass flow rates of  $H_2$ ,  $CH_4$ ,  $CO_2$ , and  $CO$  in gasification-derived syngas.

#### 4.4. The effect of gasifying agent flowrate on the composition of syngas

Steam serves as one of the gasifying agents, significantly increasing the  $H_2$  content in the syngas composition. Fig. 6 illustrates the influence of steam flowrate on the mass flowrate of syngas component and char under specific conditions of a temperature of  $900\text{ }^\circ\text{C}$  and steam flowrate ranging from 130 to 250 kg/h. Moreover, it demonstrates a clear correlation between  $H_2$  production and steam flowrate, with  $H_2$  production increasing from 22.7 to 27.34 kg/h. The higher flowrate of  $H_2$  in the syngas product array can be attributed to the promotion of water-gas (R4) and water-gas shift (R5) reactions facilitated by the presence of steam, which provides the necessary water for the water-gas shift reaction. Similarly,  $CO_2$  exhibits a similar trend due to the water-gas shift reaction (R5), rising from 2.51 to 72.26 kg/h. The mass flowrates of  $CO$  and  $CH_4$  also experience an increase with a higher steam rate. However, once they reach their maximum at approximately 138 kg/h, they start to decline with steam flowrate increase. The synergistic effect of steam as a reactant further enhances the water-gas shift reaction, as steam provides the essential  $H_2O$  required for the reaction. This cooperative influence of temperature and steam flowrate collectively contributes to the observed rise in both  $H_2$  and  $CO_2$  yields with increasing temperature.

#### 4.5. The effect of gasification temperature and pressure on cold gas efficiency

CGE is a crucial factor in evaluating system performance. As depicted in Fig. 7, CGE exhibits variations with operating parameters. The decrease in  $CO_2$  and the increase in  $CO$  are attributed to the Boudouard (R6) reaction, generating high-quality syngas at elevated temperatures. Consequently, CGE, directly linked to LHV according to Eq. (5), demonstrates an increase with rising temperatures, as observed in Fig. 7.

CGE closely aligns with the syngas LHV trend, given a constant feeding rate for each temperature. Among the gasification configurations, PP attains the maximum CGE (around 37 % at  $1200\text{ }^\circ\text{C}$ ), while 2P3S and PS exhibit CGEs of approximately 35 % and 31 % at  $1200\text{ }^\circ\text{C}$ , respectively. Similarly, the variation in CGE in Fig. 7 is directly correlated with changes in LHV. CGE diminishes with increasing pressure, with PP achieving the maximum CGE (about 36 % at 2 bars), while PS records the minimum CGE (about 30 % at 2 bars). The higher fraction of combustible gases in syngas during PP gasification contributes to the superior CGE observed in these instances compared to PS.

#### 4.6. Feature analysis of ML models

In RF, the  $R^2$  trend of the training samples demonstrates a consistent pattern, reaching a plateau close to 1. This indicates a strong correspondence between the predicted and observed values, suggesting that the model effectively captures the inherent patterns and connections within the training data. Conversely, the  $R^2$  line for the test samples initially improves as the number of data points increases, but the rate of improvement gradually slows down, converging towards the  $R^2$  value observed in the training samples. The training and test samples show a decrease in the Normalized Root Mean Square Error as the sample size increases. The NRMSE for the training sample consistently decreases, eventually reaching below 0.01, indicating a high level of predictive accuracy for the training data. The NRMSE for the test sample follows a consistent pattern, starting with a maximum value of 0.08 and progressively decreasing as more samples are included. Around 80 data points, the test sample NRMSE reaches 0.01, indicating a close alignment with the performance of the training sample. In ANN, the NRMSE error consistently decreases to below 0.1 in the training and testing datasets. The  $R^2$  term shows an increasing trend, peaking at 0.9917 with 80 samples. However, there is a minor fluctuation in the  $R^2$  values, which can be attributed to factors such as dataset complexity, noise or outliers, or non-linear relationships. Comparison of ML models and their predictive performance as presented in Table 6.

In the Gradient Boosting Regression (GBR) model, the graph of NRMSE shows that the training error initially increases and then fluctuates around 0.02. On the other hand, the testing error decreases and fluctuates around the same value. In the graph of the  $R^2$  values, the training  $R^2$  values decrease below one, while the testing  $R^2$  values increase until they reach the size of the training sample. Afterwards, both the training and testing  $R^2$  values fluctuate around a similar number, with the testing  $R^2$  slightly lower than the training  $R^2$ . These fluctuations, especially in the testing data, indicate instability in the model's performance. As for the performance of the CART model, the NRMSE error for the test data decreases to 0.02, indicating good predictive accuracy, albeit with a slight deviation from the actual values. The  $R^2$  value for the test data increases to approximately 1, signifying that the model explains a significant portion of the variability in the target variable, approaching the level of performance observed in the training data.

When considering the precision of KNN, the NRMSE graph shows a decreasing trend for both the training and test samples, reaching values below 0.02. However, the NRMSE error for the test sample is slightly higher than that of the training sample, indicating a slightly lower predictive accuracy for unseen data. In terms of the  $R^2$  graph, both the training and test samples exhibit an increasing trend, approaching a value of 1. However, the  $R^2$  value for the training sample is higher than that of the test sample, suggesting a stronger ability to explain the variability in the target variable for the training data compared to the test data.

Regarding SVR, the NRMSE graph shows a decrease in both the training and test curves, reaching approximately 0.2. This reduction in error between the predicted and actual values implies a consistent performance of the model across both the training and testing datasets.

In the  $R^2$  graph, the training and test curves demonstrate an upward

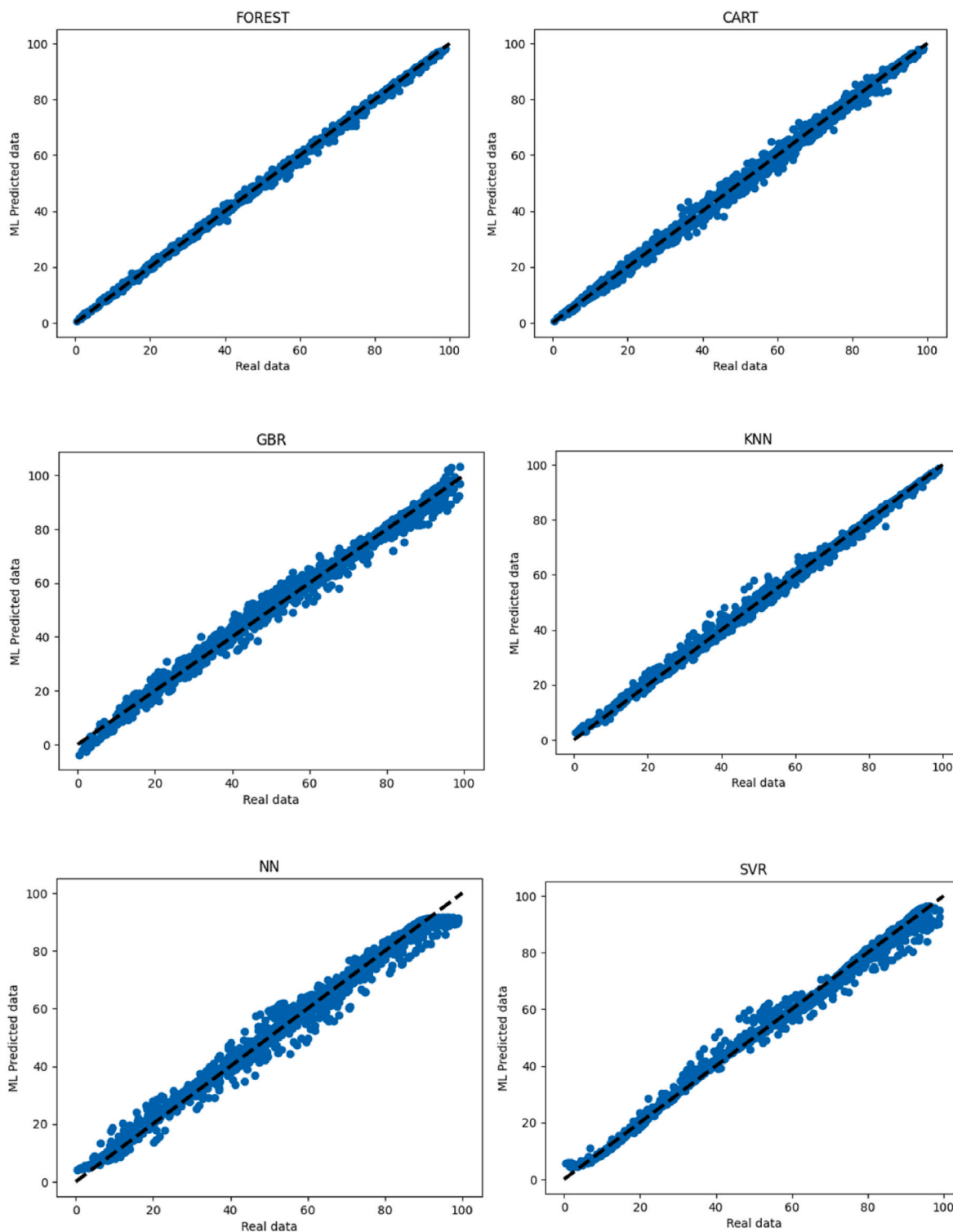


Fig. 10. The ML prediction data and real data.

trend, eventually converging to a value close to 1. This convergence signifies a robust correlation between the projected and observed values in the model. Training and testing performance evaluation of different ML algorithms in predicting the mass flow rates of main components within gasification-produced syngas, illustrated in Fig. 8.

For more clarification, a box plot which provides a visual representation of the relative performance of different ML models, assessed through the NRMSE error and  $R^2$  values [34]. Fig. 9 illustrates that the RF model outperforms both the CART and KNN models in terms of

performance, as evident from the  $R^2$  box plot. Notably, the box sizes are consistently compact across all models, indicating a consistent and minimized variability in model performance. Examining the NRMSE plot, the RF model demonstrates the most favourable performance with the lowest error value. On the other hand, the Cart and KNN models exhibit slightly higher errors, suggesting a relatively less accurate prediction capability in comparison.

Based on a careful evaluation of the established assessment criteria and the observed dispersion of data, it has been determined that the

**Table 7**  
ML model validation.

Feedstock	Inputs	Outputs	Datapoints	Highest R <sup>2</sup> value of the test	Highest accuracy ML models	Ref
Mixture of rubber and plastics	Operational conditions	H <sub>2</sub> in syngas	–	0.99	ANN	[53]
Biomass	Biomass compositions and operational conditions of gasification	H <sub>2</sub> in syngas	3500	0.99	NARXNN	[94]
Biomass	Biomass compositions and operational conditions of gasification	H <sub>2</sub> in syngas	342	0.90 0.96	RF GBR	[89]

**Table 8**  
The optimal outcome for hydrogen mass flow rate within syngas generated from gasification.

H <sub>2</sub>	Temperature of the reactor (C)	Pressure of the reactor (bar)	Mass flow rate of the gasifying agent (kg/hr)
27.81	789.65	1	250
27.78	765.52	1	250
27.77	813.79	1	250
27.7	741.38	1	250
27.69	765.52	1	244.83
27.68	789.65	1	244.83
27.65	813.79	1	244.83
27.62	837.93	1	250
27.57	741.38	1	244.8
27.53	789.65	1	239.65

utilization of RF has emerged as a significantly superior approach when compared to other models due to the high accuracy and perfectly aligned datapoints in regression analysis. This advanced methodology not only facilitates the identification and prediction of the highest output of H<sub>2</sub> gas, but also enables the determination of the optimal input conditions for achieving such outcomes. Fig. 10 presents a visual representation of the predictive accuracy pertaining to the mass flow rates of syngas, as derived from ML algorithm models. In this graphical depiction, the data points encompass both the observed actual values and the corresponding predicted values, offering a comprehensive view of their relationship. The findings indicate that, with respect to the test datasets, the RF model tends to exhibit an underestimation trend in comparison to the other algorithms. These alternative algorithms display a scattered distribution around the line of identity, suggesting that their predictions are more diverse and less systematically biased.

#### 4.7. ML model validation

The reliability of the ML models employed in this investigation has been enhanced through a comprehensive evaluation conducted to assess their accuracy. This evaluation aimed to ensure that the ML models were robust and dependable in their predictive capabilities. The utilization of distinct feedstock in conjunction with varying datasets is shown in Table 7, and it is evident that the outcomes of the model exhibit a high degree of agreement with those of alternative models. Specifically, when considering the ANN algorithm, an R<sup>2</sup> value of 0.9917 was attained during the testing phase. It is worth noting that the non-linear autoregressive with exogenous inputs neural network (NARXNN) is employed for validation due to its resemblance to ANN. Moreover, regarding RF and GBR, the achieved results closely match the research's findings. For this study, the R<sup>2</sup> values for RF and GBR were 0.9996 and 0.9963, respectively, highlighting the reliability and consistency of the outcomes.

#### 4.8. Optimization

The findings of this study are consistent with prior research, which has demonstrated a positive correlation between the temperature of the gasification reactor and the production of H<sub>2</sub> syngas [94,95]. Regarding

previous studies, the present investigation confirms that increasing the temperature of the reactor leads to a corresponding increase in the yield of H<sub>2</sub> syngas due to the enhancement in the thermochemical conversion [9]. Furthermore, it has been observed that the pyrolysis process effectively decomposes PP and PS, as the decomposition of these plastics ranges from 404 °C to 408 °C, thereby obviating the requirement for high temperatures typically associated with gasification processes [96]. This is particularly significant as high temperatures often contribute to tar formation, primarily due to the aromatic formation of plastic compounds [85]. The most favourable and optimal result for the mass flow rate of H<sub>2</sub> within syngas produced through gasification is showcased in Table 8. The specific value for the H<sub>2</sub> mass flow rate is recorded as 27.81 kg/h, as highlighted by the parameters detailed in Table 8. After the syngas undergoes a sequence of treatments involving WGS and PSA units, the ultimate yield for H<sub>2</sub> is successfully attained at 37 %, corresponding to a H<sub>2</sub> mass flow rate of 36.9 kg/h.

## 5. Conclusion

A steady-state equilibrium model was used to simulate and assess the integrated configuration encompassing pyrolysis and steam gasification procedures applied to a mixture of two waste plastic types in a 2:3 proportion (comprising 40 % PP and 60 % PS). This configuration involved WGS reactors and a PSA unit and was simulated employing the ASPEN Plus software. Employing HTWGS and LTWGS increase the H<sub>2</sub> flow rate by 30 %. The proposed model has been Validated by existing literature. The fidelity of the model was established through its congruence with documented experimental findings from the literature concerning the co-gasification of waste plastics. The congruity between the model's predictions and the empirical data remained robust for the gasification output. A sensitivity analysis was conducted to explore the influence of gasifier temperature, pressure, and steam flow rate on the composition and yield of gas products and CGS.

Utilizing the Aspen Plus platform, a gasifier model was devised to achieve data for using in ML algorithms. The applicability of ML techniques was demonstrated in their potential to optimize gasification and pyrolysis processes, and in prognosticating the yields and attributes of resultant products from these processes. Within this framework, five ML algorithms – KNN, SVR, ANN, CART, RF, and GBR – were implemented. Notably, the ML model achieved effective prognostication of the mass flow rate of syngas, as indicated by R<sup>2</sup> values ranging from 0.55 to 0.99. This success was attained after the identification of gasification parameters as model inputs. Among various models, the R<sup>2</sup> values recorded for the test and training datasets exceeded 0.99, corroborating the robustness of the RF model in foreseeing syngas composition and mass flow rate with a high degree of accuracy. This capability was achieved without necessitating intricate calculations or resource-intensive experimental inquiries. Following optimization endeavours, the final H<sub>2</sub> yield culminated at 37 %.

## Declaration of competing interest

The authors declare that they have no known competing financial interests or personal relationships that could have appeared to influence the work reported in this paper.

## References

- [1] Okati A, Khani MR, Shokri B, Monteiro E, Rouboa A. On the operating parameters for hydrogen-rich syngas production in a plasma co-gasification process of municipal solid wastes and polypropylene using a constrained model in aspen plus. *J Energy Inst* 2023;107:101173.
- [2] Chai Y, Packham N, Wang M. Process improvement analysis of pyrolysis/gasification of biomass and waste plastics with carbon capture and utilisation through process simulation. *Fuel* 2022;324:124571.
- [3] Wong SL, Ngadi N, Abdullah TAT, Inuwa IM. Current state and future prospects of plastic waste as source of fuel: a review. *Renew Sustain Energy Rev* 2015;50:1167–80.
- [4] Awogbemi O, Kallon DVV. Achieving affordable and clean energy through conversion of waste plastic to liquid fuel. *J Energy Inst* 2023;106:101154.
- [5] Zhao X, Cornish K, Vodovotz Y. Narrowing the gap for bioplastic use in food packaging: an update. *Environ Sci Technol* 2020;54(8):4712–32.
- [6] Borrelle SB, Ringma J, Law KL, Monnahan CC, Lebreton L, McGivern A, Murphy E, Jambeck J, Leonard GH, Hilleary MA. Predicted growth in plastic waste exceeds efforts to mitigate plastic pollution. *Science* 2020;369(6510):1515–8.
- [7] Cox KD, Covernton GA, Davies HL, Dower JF, Juanes F, Dudas SE. Human consumption of microplastics. *Environ Sci Technol* 2019;53(12):7068–74.
- [8] Geyer R, Jambeck JR, Law KL. Production, use, and fate of all plastics ever made. *Sci Adv* 2017;3(7):e1700782.
- [9] Li J, Burra KG, Wang Z, Liu X, Kerdsuwan S, Gupta AK. Energy recovery from composite acetate polymer-biomass wastes via pyrolysis and CO<sub>2</sub>-assisted gasification. *J Energy Resour Technol* 2021;143(4):042305.
- [10] Thakur S, Verma A, Sharma B, Chaudhary J, Tamulevicius S, Thakur VK. Recent developments in recycling of polystyrene based plastics. *Curr Opin Green Sustainable Chem* 2018;13:32–8.
- [11] Jeong Y, Kim J, Seo M, Mun T, Kim J. Characteristics of two-stage air gasification of polystyrene with active carbon as a tar removal agent. *Energy* 2021;219:119681.
- [12] Statista. Polypropylene (PP) market size in Europe in 2018 and 2019, with a forecast for 2027. Available: <https://www.statista.com/statistics/1272614/polypropylene-market-size-europe/>. [Accessed 20 June 2023].
- [13] HajjiHashemi M, Mazhkoo S, Dadfar H, Livani E, Naseri Varnosefaderani A, Pourali O, Najafi Nobar S, Dutta A. Combined heat and power production in a pilot-scale biomass gasification system: experimental study and kinetic simulation using ASPEN plus. *Energy* 2023;276:127506.
- [14] Caputo AC, Palumbo M, Pelagagge PM, Scacchia F. Economics of biomass energy utilization in combustion and gasification plants: effects of logistic variables. *Biomass Bioenergy* 2005;28(1):35–51.
- [15] Saebea D, Ruengrit P, Arpornwichanop A, Patcharavorachot Y. Gasification of plastic waste for synthesis gas production. *Energy Rep* 2020;6:202–7.
- [16] Burra KG, Gupta AK. Kinetics of synergistic effects in co-pyrolysis of biomass with plastic wastes. *Appl Energy* 2018;220:408–18.
- [17] Kamireddi D, Therapalli A, Sridevi V, Bai MT, Surya DV, Rao CS, Jeeru LR. Microwave-assisted in-situ catalytic co-pyrolysis of polypropylene and polystyrene mixtures: response surface methodology analysis using machine learning. *J Anal Appl Pyroly* 2023;172:105984.
- [18] Li J, Ye X, Burra KG, Lu W, Wang Z, Liu X, Gupta AK. Synergistic effects during co-pyrolysis and co-gasification of polypropylene and polystyrene. *Appl Energy* 2023;336:120750.
- [19] Bin Abu Sofian ADA, Lim HR, Chew KW, Khoo KS, Tan IS, Ma Z, Show PL. Hydrogen production and pollution mitigation: enhanced gasification of plastic waste and biomass with machine learning & storage for a sustainable future. *Environ Pollut* 2024;342:123024.
- [20] Chai Y, Gao N, Wang M, Wu C. H<sub>2</sub> production from co-pyrolysis/gasification of waste plastics and biomass under novel catalyst ni-CaO-C. *Chem Eng J* 2020;382:122947.
- [21] Cardoso J, Silva V, Eusébio D. Techno-economic analysis of a biomass gasification power plant dealing with forestry residues blends for electricity production in Portugal. *J Clean Prod* 2019;212:741–53.
- [22] Ram M, Mondal MK. Chapter 13 - biomass gasification: a step toward cleaner fuel and chemicals. In: Gurunathan Baskar, Sahadevan Renganathan, Zakaria Zainul Akmar, editors. *Biofuels and bioenergy*. Elsevier; 2022. p. 253–76.
- [23] Tezer Ö, Karabag N, Öngen A, Çolpan CÖ, Ayol A. Biomass gasification for sustainable energy production: a review. *Int J Hydrogen Energy* 2022;47(34):15419–33.
- [24] Ermolaev DV, Karaeva JV, Timofeeva SS, Kovalev AA, Kovalev DA, Littl YV. Modeling of air gasification of dark fermentation digestate in a downdraft gasifier. *Int J Hydrogen Energy* 2023;48(63):24255–63.
- [25] Vikram S, Deore SP, De Blasio C, Mahajani SM, Kumar S. Air gasification of high-ash solid waste in a pilot-scale downdraft gasifier: experimental and numerical analysis. *Energy* 2023;126912.
- [26] Burra KG, Gupta AK. Synergistic effects in steam gasification of combined biomass and plastic waste mixtures. *Appl Energy* 2018;211:230–6.
- [27] Ma Y, Ge Z, Zeng M, Zha Z, Tao Y, Zhang H. Reactivity and performance of steam gasification during biomass batch feeding. *Carbon Resources Conversion* 2023;6(3):229–37.
- [28] Wilk V, Hofbauer H. Conversion of mixed plastic wastes in a dual fluidized bed steam gasifier. *Fuel* 2013;107:787–99.
- [29] Liao M, Wang C, Weng J, Xu L, Shu R, Du Y, Chen Y, Song Q, Tian Z. H<sub>2</sub>-rich gas production from wood biomass air-steam gasification over a multifunctional Ni<sub>1.5</sub>Ca<sub>4.0</sub>Mn<sub>1.0</sub>O<sub>x</sub> catalyst derived from biomaterial. *Fuel Process Technol* 2023;249:107848.
- [30] Kakati U, Sakhiya AK, Baghel P, Trada A, Mahapatra S, Upadhyay D, Kaushal P. Sustainable utilization of bamboo through air-steam gasification in downdraft gasifier: experimental and simulation approach. *Energy* 2022;252:124055.
- [31] Schmid M, Schmidberger C, Scheffknecht G. Modelling and simulation of fluidized bed steam-oxygen gasification of sewage sludge using thermochemical equilibrium and experimental data. *Fuel* 2023;341:127595.
- [32] Kaydoun M, El Hassan N. Thermodynamic simulation of the co-gasification of biomass and plastic waste for hydrogen-rich syngas production. *Results in Engineering* 2022;16:100771.
- [33] Basha MH, Sulaiman SA, Uemura Y. Co-gasification of palm kernel shell and polystyrene plastic: effect of different operating conditions. *J Energy Inst* 2020;93(3):1045–52.
- [34] Abioye KJ, Harun NY, Sufian S, Yusuf M, Jagaba AH, Waqas S, Ayodele BV, Kamyab H, Alam M, Gupta M, Gill HS, Reznia S, Chelliapan S, Kang K. Optimization of syngas production from co-gasification of palm oil decanter cake and alum sludge: an RSM approach with char characterization. *Environ Res* 2024;246:118027.
- [35] Murugan PC, Joseph Sekhar S, Glivin G, Saji Raveendran P, Le T, Mathimani T. Investigation on thermochemical co-gasification of rice husk and groundnut shell in open core gasifier for the generation of producer gas: an optimization by central composite design. *Environ Res* 2024;242:117741.
- [36] Zallaya S, El Achkar JH, Chacra AA, Shatila S, El Akhdar J, Daher Y. Steam gasification modeling of polyethylene (PE) and polyethylene terephthalate (PET) wastes: a case study. *Chem Eng Sci* 2023;267:118340.
- [37] Yang Q, Zhang J, Zhou J, Zhao L, Zhang D. A hybrid data-driven machine learning framework for predicting the performance of coal and biomass gasification processes. *Fuel* 2023;346:128338.
- [38] Mojaver M, Hasanazadeh R, Azdast T, Park CB. Comparative study on air gasification of plastic waste and conventional biomass based on coupling of AHP/TOPSIS multi-criteria decision analysis. *Chemosphere* 2022;286:131867.
- [39] The limits of biomass. *One Earth* 2022;5(1):1–2. <https://doi.org/10.1016/j.oneear.2022.01.001>.
- [40] Faraji M, Saidi M. Hydrogen-rich syngas production via integrated configuration of pyrolysis and air gasification processes of various algal biomass: process simulation and evaluation using aspen plus software. *Int J Hydrogen Energy* 2021;46(36):18844–56.
- [41] Mahmood A, Wang J. Machine learning for high performance organic solar cells: current scenario and future prospects. *Energy Environ Sci* 2021;14(1):90–105.
- [42] Mutlu AY, Yucel O. An artificial intelligence based approach to predicting syngas composition for downdraft biomass gasification. *Energy* 2018;165:895–901.
- [43] Tang Q, Chen Y, Yang H, Liu M, Xiao H, Wu Z, Chen H, Naqvi SR. Prediction of bio-oil yield and hydrogen contents based on machine learning method: effect of biomass compositions and pyrolysis conditions. *Energy Fuels* 2020;34(9):11050–60.
- [44] Ullah Z, Khan M, Naqvi SR, Khan MNA, Farooq W, Anjum MW, Yaqub MW, AlMohamadi H, Almomani F. An integrated framework of data-driven, metaheuristic, and mechanistic modeling approach for biomass pyrolysis. *Process Saf Environ Protect* 2022;162:337–45.
- [45] Yang Y, Shahbeik H, Shafizadeh A, Rafiee S, Hafezi A, Du X, Pan J, Tabatabaei M, Aghbashlo M. Predicting municipal solid waste gasification using machine learning: a step toward sustainable regional planning. *Energy* 2023;278:127881.
- [46] Khan M, Ullah Z, Mašek O, Naqvi SR, Khan MNA. Artificial neural networks for the prediction of biochar yield: a comparative study of metaheuristic algorithms. *Bioresour Technol* 2022;355:127215.
- [47] Mu L, Wang Z, Wu D, Zhao L, Yin H. Prediction and evaluation of fuel properties of hydrochar from waste solid biomass: machine learning algorithm based on proposed PSO-NN model. *Fuel* 2022;318:123644.
- [48] Li X, Zhong K, Feng L. Machine learning-based metaheuristic optimization of an integrated biomass gasification cycle for fuel and cooling production. *Fuel* 2023;332:125969.
- [49] Kim JY, Kim D, Li ZJ, Dariva C, Cao Y, Ellis N. Predicting and optimizing syngas production from fluidized bed biomass gasifiers: a machine learning approach. *Energy* 2023;263:125900.
- [50] Fang Yi, Ma Li, Yao Zhiyi, Li Wangliang, You Siming. Process optimization of biomass gasification with a Monte Carlo approach and random forest algorithm. *Energy Convers Manag* 2022;264:115734.
- [51] Hai T, Ashraf Ali M, Zhou J, Dhahad HA, Goyal V, Fahad Almojil S, Ibrahim Almohana A, Fahmi Alali A, Twfiq Almoalimi K, Najat Ahmed A. Feasibility and environmental assessments of a biomass gasification-based cycle next to optimization of its performance using artificial intelligence machine learning methods. *Fuel* 2023;334:126494.
- [52] Mojaver M, Azdast T, Hasanazadeh R. Assessments of key features and taguchi analysis on hydrogen rich syngas production via gasification of polyethylene, polypropylene, polycarbonate and polyethylene terephthalate wastes. *Int J Hydrogen Energy* 2021;46(58):29846–57.
- [53] Ayodele B, Mustapa S, Kanthasamy R, Zwawi M, Cheng C. Modeling the prediction of hydrogen production by co-gasification of plastic and rubber wastes using machine learning algorithms. *Int J Energy Res* 2021;45.
- [54] Cheng Y, Ekici E, Yildiz G, Yang Y, Coward B, Wang J. Applied machine learning for prediction of waste plastic pyrolysis towards valuable fuel and chemicals production. *J Anal Appl Pyroly* 2023;169:105857.
- [55] Hasanazadeh R, Mojaver P, Azdast T, Khalilarya S, Chitsaz A. Developing gasification process of polyethylene waste by utilization of response surface methodology as a machine learning technique and multi-objective optimizer approach. *Int J Hydrogen Energy* 2023;48(15):5873–86.

- [56] Saravanan A, Parida S, Murugan M, Reddy MS, Elumalai PV, Kumar Dash S. Thermal performance prediction of a solar air heater with a C-shape finned absorber plate using RF, LR and KNN models of machine learning. *Therm Sci Eng Prog* 2023;38:101630.
- [57] Breiman L. Random forests. *Mach Learn* 2001;45:5–32.
- [58] İskenderoğlu FC, Baltacıoğlu MK, Demir MH, Baldinelli A, Borelli L, Bidini G. Comparison of support vector regression and random forest algorithms for estimating the SOFC output voltage by considering hydrogen flow rates. *Int J Hydrogen Energy* 2020;45(60):35023–38.
- [59] Lei C, Deng J, Cao K, Ma L, Xiao Y, Ren L. A random forest approach for predicting coal spontaneous combustion. *Fuel* 2018;223:63–73.
- [60] Pandey DS, Raza H, Bhattacharyya S. Development of explainable AI-based predictive models for bubbling fluidised bed gasification process. *Fuel* 2023;351:128971.
- [61] Shafizadeh A, Shahbeig H, Nadian MH, Mobli H, Dowlati M, Gupta VK, Peng W, Lam SS, Tabatabaei M, Aghbashlo M. Machine learning predicts and optimizes hydrothermal liquefaction of biomass. *Chem Eng J* 2022;445:136579.
- [62] Xiao G, Ni M, Chi Y, Jin B, Xiao R, Zhong Z, Huang Y. Gasification characteristics of MSW and an ANN prediction model. *Waste Manag* 2009;29(1):240–4.
- [63] Hasan N, Chaudhary K, Alam M. Unsupervised machine learning framework for early machine failure detection in an industry. *J Discrete Math Sci Cryptogr* 2021;24(5):1497–508.
- [64] Amar MN, Shateri M, Hemmati-Sarapardeh A, Alamatsaz A. Modeling oil-brine interfacial tension at high pressure and high salinity conditions. *J Petrol Sci Eng* 2019;183:106413.
- [65] Noori R, Abdoli MA, Ghasrodashti AA, Jalili Ghazizade M. Prediction of municipal solid waste generation with combination of support vector machine and principal component analysis: a case study of mashhad. *Environ Prog Sustain Energy: An Official Publication of the American Institute of Chemical Engineers* 2009;28(2): 249–58.
- [66] Umenweke GC, Afolabi IC, Epelle EI, Okolie JA. Machine learning methods for modeling conventional and hydrothermal gasification of waste biomass: a review, vol. 17. *Bioresour Technol Reports*; 2022, 100976.
- [67] Hosseinzadeh A, Zhou JL, Altaee A, Li D. Machine learning modeling and analysis of biohydrogen production from wastewater by dark fermentation process. *Bioresour Technol* 2022;343:126111.
- [68] Motevalizadeh SM, Kavussi A, Mollenhauer K. Predicting the fracture mechanics responses of recycled asphalt mixes using machine learning-based algorithms: application of CART algorithm and neural networks. *Eng Fract Mech* 2022;276: 108791.
- [69] Bevilacqua M, Braglia M, Montanari R. The classification and regression tree approach to pump failure rate analysis. *Reliab Eng Syst Saf* 2003;79(1):59–67.
- [70] Hu X, Shentu J, Xie N, Huang Y, Lei G, Hu H, et al. Predicting triaxial compressive strength of high-temperature treated rock using machine learning techniques. *J Rock Mech Geotech Eng* 2022;15(8):2072–82.
- [71] Ma Z, Wang J, Feng Y, Wang R, Zhao Z, Chen H. Supercritical water gasification of organic solid waste: H<sub>2</sub> yield and cold gas efficiency optimization considering modeling uncertainties. *Int J Hydrogen Energy* 2023;48(79):30702–17.
- [72] Ozbas EE, Aksu D, Ongen A, Aydin MA, Ozcan HK. Hydrogen production via biomass gasification, and modeling by supervised machine learning algorithms. *Int J Hydrogen Energy* 2019;44(32):17260–8.
- [73] Fathabadi A, Seyedian SM, Malekian A. Comparison of bayesian, k-nearest neighbor and Gaussian process regression methods for quantifying uncertainty of suspended sediment concentration prediction. *Sci Total Environ* 2022;818:151760.
- [74] Liu S, Yang Y, Yu L, Zhu F, Cao Y, Liu X, Yao A, Cao Y. Predicting gas production by supercritical water gasification of coal using machine learning. *Fuel* 2022;329: 125478.
- [75] Gaye B, Zhang D, Wulamu A. Improvement of support vector machine algorithm in big data background. *Math Probl Eng* 2021:1–9. 2021.
- [76] Terry LM, Wee MXJ, Chew JJ, Khaerudini DS, Timuda GE, Aqsha A, Saptoro A, Sunarso J. Co-pyrolysis of oil palm trunk and polypropylene: pyrolysis oil composition and formation mechanism. *S Afr J Chem Eng* 2023;43:348–58.
- [77] Adeboye BS, Adewole BZ, Adedaja AM, Obayopo SO, Asere AA, Kayode O, Idris MO, Okediran IK. Optimization and modeling of process parameters on the yield of enhanced pyrolysis oil during co-pyrolysis of cassava peel with polystyrene. *Environmental Challenges* 2021;5:100347.
- [78] Singh M, Salaudeen SA, Gilroyed BH, Dutta A. Simulation of biomass-plastic co-gasification in a fluidized bed reactor using aspen plus. *Fuel* 2022;319:123708.
- [79] Chalermisinsuwan B, Li Y, Manatura K. Optimization of gasification process parameters for COVID-19 medical masks using response surface methodology. *Alex Eng J* 2023;62:335–47.
- [80] Parthasarathy P, Narayanan KS. Hydrogen production from steam gasification of biomass: influence of process parameters on hydrogen yield – a review, vol. 66. *Renewable Energy*; 2014. p. 570–9.
- [81] Ajorloo M, Ghodrat M, Scott J, Strezov V. Modelling and statistical analysis of plastic biomass mixture co-gasification. *Energy* 2022;256:124638.
- [82] Marcantonio V, Bocci E, Ouweltjes JP, Del Zotto L, Monarca D. Evaluation of sorbents for high temperature removal of tars, hydrogen sulphide, hydrogen chloride and ammonia from biomass-derived syngas by using aspen plus. *Int J Hydrogen Energy* 2020;45(11):6651–62.
- [83] Detchusananard T, Wuttipisan N, Limleamthong P, Prasertcharoensuk P, Maréchal F, Arpornwichanop A. Pyrolysis and gasification integrated process of empty fruit bunch for multi-biofuels production: technical and economic analyses. *Energy Convers Manag* 2022;258:115465.
- [84] Marcantonio V, De Falco M, Capocelli M, Bocci E, Colantoni A, Villarini M. Process analysis of hydrogen production from biomass gasification in fluidized bed reactor with different separation systems. *Int J Hydrogen Energy* 2019;44(21):10350–60.
- [85] Doherty W, Reynolds A, Kennedy D. The effect of air preheating in a biomass CFB gasifier using ASPEN plus simulation. *Biomass Bioenergy* 2009;33(9):1158–67.
- [86] Guan J, Huang T, Liu W, Feng F, Japip S, Li J, Wu J, Wang X, Zhang S. Design and prediction of metal organic framework-based mixed matrix membranes for CO<sub>2</sub> capture via machine learning. *Cell Reports Physical Science* 2022;3(5):100864.
- [87] Yang X, Yuan C, He S, Jiang D, Cao B, Wang S. Machine learning prediction of specific capacitance in biomass derived carbon materials: effects of activation and biochar characteristics. *Fuel* 2023;331:125718.
- [88] Wang D, Cao R, Hao S, Liang C, Chen G, Chen P, Li Y, Zou X. Accelerated prediction of Cu-based single-atom alloy catalysts for CO<sub>2</sub> reduction by machine learning. *Green Energy & Environment*; 2021.
- [89] Li J, Li L, Tong YW, Wang X. Understanding and optimizing the gasification of biomass waste with machine learning. *Green Chemical Engineering* 2023;4(1): 123–33.
- [90] Onsree T, Tippayawong N. Machine learning application to predict yields of solid products from biomass torrefaction. *Renew Energy* 2021;167:425–32.
- [91] Sison AE, Etchieson SA, Güleç F, Epelle EI, Okolie JA. Process modelling integrated with interpretable machine learning for predicting hydrogen and char yield during chemical looping gasification. *J Clean Prod* 2023;414:137579.
- [92] Katongtung T, Onsree T, Tippayawong N. Machine learning prediction of biocrude yields and higher heating values from hydrothermal liquefaction of wet biomass and wastes. *Bioresour Technol* 2022;344:126278.
- [93] Njuguna F, Ndiritu H, Gathitu B, Hawi M, Munyalo J. Kinetic modeling and optimization of process parameters for gasification of macadamia nutshells with air preheating: a combined use of aspen plus and response surface methodology (RSM) vol. 22. *Bioresour Technol Reports*; 2023, 101477.
- [94] Elmaz F, Yücel Ö. Data-driven identification and model predictive control of biomass gasification process for maximum energy production. *Energy* 2020;195: 117037.
- [95] Kim J, Mun T, Kim J, Kim J. Air gasification of mixed plastic wastes using a two-stage gasifier for the production of producer gas with low tar and a high calorific value. *Fuel* 2011;90(6):2266–72.
- [96] Bai B, Wang W, Jin H. Experimental study on gasification performance of polypropylene (PP) plastics in supercritical water. *Energy* 2020;191:116527.